Engineering enhanced thermoelectric properties in zigzag graphene nanoribbons

Hossein Karamitaheri,[1,2,a)] Neophytos Neophytou,[1] Mahdi Pourfath,[3,1] Rahim Faez,[2] and Hans Kosina[1]
[1]*Institute for Microelectronics, Technische Universitat Wien, Gusshausstrasse 27-29/E360, A-1040 Wien, Austria*
[2]*School of Electrical Engineering, Sharif University of Technology, Tehran 11365-9363, Iran*
[3]*Electrical and Computer Engineering Department, University of Tehran, Tehran 14395-515, Iran*

(Received 16 September 2011; accepted 28 January 2012; published online 1 March 2012)

We theoretically investigate the thermoelectric properties of zigzag graphene nanoribbons in the presence of extended line defects, substrate impurities, and edge roughness along the nanoribbon's length. A nearest-neighbor tight-binding model for the electronic structure and a fourth nearest-neighbor force constant model for the phonon bandstructure are used. For transport, we employ quantum mechanical non-equilibrium Green's function simulations. Starting from the pristine zigzag nanoribbon structure that exhibits very poor thermoelectric performance, we demonstrate how after a series of engineering design steps the performance can be largely enhanced. Our results could be useful in the design of highly efficient nanostructured graphene nanoribbon–based thermoelectric devices. © *2012 American Institute of Physics*. [http://dx.doi.org/10.1063/1.3688034]

I. INTRODUCTION

The ability of a material to convert heat into electricity is measured by the dimensionless thermoelectric figure of merit ZT defined by

$$ZT = \frac{S^2GT}{(\kappa_e + \kappa_l)}, \quad (1)$$

where S denotes the Seebeck coefficient, G the electrical conductance, T the temperature, κ_e the electronic, and κ_l the lattice parts of the thermal conductance.[1] Due to the strong interconnection between the parameters that control ZT, it has been traditionally proven difficult to achieve values above unity, which translates to low conversion efficiencies and limits the applications for thermoelectricity.

The recent advancements in lithography and nanofabrication, however, have led to the realization of breakthrough experiments on nanostructured thermoelectric devices that demonstrated enhanced performance, sometimes even up to 2 orders of magnitude higher than the corresponding bulk material values. Nanostructures provided the possibility of independently designing the quantities that control the ZT in achieving higher values. Enhanced performance was demonstrated for 1D nanowires (NWs),[2,3] 2D thin films, 1D/2D superlattices,[4,5] as well as materials with embedded nanostructuring.[6]

Graphene, a recently discovered two-dimensional form of carbon, has received much attention over the past few years due to its excellent electrical, optical, and thermal properties.[7] Graphene, however, is not a useful thermoelectric material. Although its electrical conductance is as high as that of copper,[8] its ability to conduct heat is even higher,[9] which increases the denominator of ZT. To make things worse, as a zero bandgap material, pristine graphene has a very small Seebeck coefficient,[10] which minimizes the power factor S^2G. Nanoengineering, however, could provide ways to increase the Seebeck coefficient and decrease the thermal conductivity as well.

The high thermal conductivity of graphene is mostly due to the lattice contribution, whereas the electronic contribution to the thermal conduction is smaller.[11,12] In order to reduce the thermal conductivity, therefore, the focus is placed on reducing phonon conduction. Recently, many theoretical studies have been performed regarding the thermal conductivity of graphene-based structures. Several methods, such as the introduction of vacancies, defects, isotope doping, edge roughness, and boundary scattering, can considerably reduce thermal conductance.[13–15] Importantly, in certain instances, this can be achieved without significant reduction of the electrical conductance.

In order to improve the Seebeck coefficient, graphene needs to acquire a bandgap. This can be achieved by appropriate patterning of the graphene sheet into nanoribbons.[16,17] Graphene nanoribbons (GNRs) are thin strips of graphene, where the bandgap depends on the chirality of the edges (armchair or zigzag) and the width of the ribbon. Armchair GNRs (AGNRs) can be semiconductors with a bandgap inversely proportional to their width.[16] Although the acquired bandgap can increase the Seebeck coefficient, when attempting to reduce the thermal conductivity by introducing disorder in the nanoribbon, as described above, the electrical conductivity is also strongly affected[18,19] and the thermoelectric performance remains low. Zigzag GNRs (ZGNRs), on the other hand, show metallic behavior with very low Seebeck coefficient, but, as described in Ref. 19, the transport in ZGNRs is nearly unaffected in the presence of line edge roughness, at least in the first conduction plateau around their Fermi level.

In this work, by using atomistic electronic and phononic bandstructure calculations and quantum mechanical transport simulation, we show that, despite the zero bandgap, the thermoelectric performance of ZGNRs can be largely enhanced.

a)Author to whom correspondence should be addressed. Electronic mail: karami@iue.tuwien.ac.at.

For this, a series of design steps are employed: i) Introducing extended line defects (ELDs), as described in Ref. 20, can break the symmetry between electrons and holes by adding additional electronic bands. This practically provides a sharp band edge around the Fermi level and offers a band asymmetry, which, for thermoelectric purposes, practically constitutes an "effective bandgap". ii) Introducing background impurities enhances the "effective bandgap". iii) Introducing edge roughness reduces the lattice part of the thermal conductivity (significantly more than it reduces the electrical conductivity). After such a procedure, we demonstrate that the figure of merit ZT can be greatly enhanced and high thermoelectric performance could be achieved.

The paper is organized as follows: In Sec. II, we describe the methodology used in our calculations. In Sec. III, we present the results for the electronic/phononic structure and transmission of ZGNRs for every step of our design approach (in Sec. III A) and their influence on the thermoelectric coefficients (in Sec. III B). Finally, in Sec. IV, we conclude.

II. APPROACH

In the linear response regime, the transport coefficients can be evaluated using the Landauer formula,[21–23]

$$G = \left(\frac{2q^2}{h}\right) I_0 \quad [1/\Omega], \tag{2}$$

$$S = \left(-\frac{k_B}{q}\right) \frac{I_1}{I_0} \quad [V/K], \tag{3}$$

$$\kappa_e = \left(\frac{2T\,k_B^2}{h}\right) \left[I_2 - \frac{I_1^2}{I_0}\right] \quad [W/K]. \tag{4}$$

Here, h is the Planck constant, k_B is the Boltzmann constant, and

$$I_j = \int_{-\infty}^{+\infty} \left(\frac{E - E_F}{k_B T}\right)^j T_{el}(E) \left(-\frac{\partial f}{\partial E}\right) dE, \tag{5}$$

where $T_{el}(E)$ is the electronic transmission probability, $f(E)$ is the Fermi function, and E_F is the Fermi level of the system. Similarly, the lattice contribution to the thermal conductance can be given as a function of the phonon transmission probability,[18]

$$\kappa_l = \frac{1}{h} \int_0^{+\infty} T_{ph}(\omega) \hbar\omega \left(\frac{\partial n(\omega)}{\partial T}\right) d(\hbar\omega), \tag{6}$$

where $n(\omega)$ denotes the Bose-Einstein distribution function and $T_{ph}(\omega)$ is the phonon transmission probability.[24]

For the electronic structure, the Hamiltonian of the GNRs is described in the standard first nearest-neighbor atomistic tight-binding p_z orbital approximation. The hopping parameter is set to –2.7 eV, and the on-site potential is shifted to zero so that the Fermi level remains at 0 eV. This model has been recently used to describe the electronic transport of ELD-ZGNR with double- vacancies, and the results are in good agreement with first-principle calculations and experimental studies.[20,25] To the best of our knowledge, only a few first-principle calculations and experimental studies have been conducted in structures that include ELDs.[25–27] The two main features of the electronic structure, the asymmetry between electrons and holes, and the metallic behavior of the ELD in the graphene ribbon channel have been described in these studies and are also captured by the tight-binding model, as we will demonstrate below.

For the phonon modes, the dynamic matrix is constructed using the fourth nearest-neighbor force constant model.[23] The force constant method uses a set of empirical fitting parameters and can be easily calibrated to experimental measurements. We use the fitting parameters given in Ref. 28 for graphene-based structures. We assume that this model is still valid under structures that include ELDs. Although verification of its validity for ELD-ZGNRs has not been demonstrated yet, i.e. using first-principle calculations, in Ref. 29, it was shown using DFT simulations that there is little difference between the phonon transmissions of carbon nanotube structures with/without ELDs, which could justify our model choice. In any case, as we show below, the main influence on the phonon transport in this work originates from edge roughness scattering, which reduces the phonon transmission drastically. The effect of edge roughness scattering is the dominant effect, and that can be captured adequately by the model we employ in this work. The influence of the ELDs on the phonon transmission is much smaller compared to the effect of the edge roughness, and therefore, we still choose to use the numerically less expensive fourth nearest-neighbor force constant method.

In this work, the fully quantum mechanical nonequilibrium Green's function formalism (NEGF) is used for transport calculations of both electrons and phonons. The system geometry is defined as a set of two semi-infinite contacts and a channel (device) with length L. The device Green's function is obtained as

$$G_{el}(E) = \left(EI - H - \Sigma_{s,el} - \Sigma_{d,el}\right)^{-1} \tag{7}$$

for electron calculation, where H is the device Hamiltonian matrix and E is the energy. In the case of phonon transport, the Green's function is given by

$$G_{ph}(E) = \left(EI - D - \Sigma_{s,ph} - \Sigma_{d,ph}\right)^{-1}, \tag{8}$$

where D is the dynamic matrix and $E = \hbar\omega$.[30] The contact self-energy matrices $\sum_{s/d}$ are calculated using the Sancho-Rubio iterative scheme.[31] The effective transmission probability through the channel can be achieved using the relation

$$T_{el/ph}(E) = \mathrm{Trace}[\Gamma_s G \Gamma_d G^\dagger], \tag{9}$$

where Γ_s and Γ_d are the broadening functions of contacts.[32]

This method is very effective in describing the effect of realistic distortion in nanostructures, including all quantum mechanical effects. In our calculation, we include long-range substrate impurities with density of one impurity per 125 nm and edge distortion (roughness) up to four layers in each side of the ribbon's edge. These are applied only on the device part and not in the contact regions.[19]

III. RESULTS AND DISCUSSION

An efficient thermoelectric material must be able to effectively separate hot from cold carriers. The quantity that determines the ability to filter carriers is the Seebeck coefficient. The Seebeck coefficient depends on the asymmetry of the density of states around the Fermi level. In a semiconductor the Seebeck coefficient is large, but in a metal where the density of states is more uniform in energy the Seebeck coefficient is small. Metallic ZGNRs also have a small Seebeck coefficient, because their transmission is constant around the Fermi level, despite the peak in the DOS at $E=0$ eV due to the edge states. Recently, however, Bahamon *et al.* have investigated the electrical properties of ZGNRs that included an ELD (ELD-ZGNRs) along the nanoribbon's length.[20] It was reported that the ELD breaks the electron-hole energy symmetry in nanoribbons and introduces an additional electron band around the Fermi level. In such a way, an asymmetry in the density of states and the transmission function are achieved, which improves the Seebeck coefficient, as we will show further down. This particular structure has also been recently experimentally realized.[25] Although the method of fabrication was rather complicated to be able to scale for industrial applications, nevertheless, it makes studies on GNRs appropriate and interesting as well.

A. Electronic and phononic structure

The changes in the electronic structure of the ZGNRs after the introduction of the ELD are demonstrated in Fig. 1. Figure 1(a) shows the atomistic geometry of the pristine ZGNR of width $W \sim 4$ nm (with 20 zigzag edge lines) and Fig. 1(b) its electronic structure. The Fermi level is at $E=0$ eV, due to the symmetry between electron and hole bands. Figure 1(c) shows the structure of the ELD-ZGNR with the same width. The region in which the ELD is introduced is shown in the middle (in red). The ELD changes the hexagons of the GNR to pentagons and octagons after a local rearrangement of the bonding and the introduction of two additional atoms in the unit cell. We use a two parameter notation to describe the ELD-ZGNR structure throughout this work as ELD-ZGNR(n_1, n_2), where n_1 and n_2 are the indices of the partial-ZGNRs above and below the line defect, respectively (i.e., the number of zigzag edge lines of atoms), although, in all cases, we use $n_1=n_2$. The band structure of the ELD-ZGNR(10,10) is shown in Fig. 1(d). The thick line (in red) shows a new band that is introduced in the conduction band near the Fermi energy ($E=0$ eV), which corresponds to the ELD. There are two points that result in the creation of the extra band. Part of the physics behind this is explained by Pereira *et al.* in Ref. 33. The first point is that a defect in the graphene system will introduce states that reside close to the Fermi level at $E=0$ eV. This is similar to the edge states of the ribbons that tend to reside near the Fermi level. The second point, again described in Ref. 33, is that an asymmetry in the dispersion between electrons and holes will be created when carbon atoms of the graphene sublattice "A" (or "B") are coupled with atoms from "A" (or "B") again. Usually, the atomic arrangement in graphene can be split into sublattices "A" and "B", where

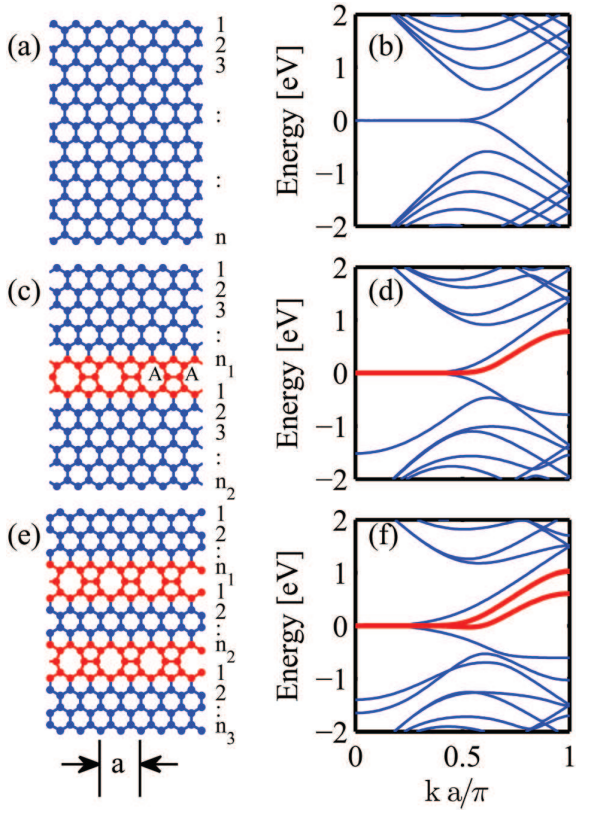

FIG. 1. (Color online) The geometrical structure of (a) ZGNR(n), (c) ELD-ZGNR(n_1,n_2), and (e) 2ELD- ZGNR(n_1,n_2,n_3). The band structure of (b) ZGNR(20), (d) ELD-ZGNR(10,10), and (f) 2ELD- ZGNR(8,4,8). The band structure of ZGNR(20) is folded for a better comparison. The translation vector length is $a=0.49$ nm. The n, n_1, n_2, and n_3 indicate the number of zigzag edges on the top, bottom, and middle of the ELD regions, as indicated.

atoms from "A" couple to "B" and vice versa. When this happens, the dispersion is symmetric in the first-nearest neighbor tight-binding model. At a defect side, such as the ELD we consider, where "A" connects to "A" as seen in Fig. 1(c), such asymmetry can be observed. The fact that the overall bandstructure has additional bands compared to the pristine ribbon is also connected to the two extra atoms in the unit cell.

Moving one step further, in Fig. 1(e), we show the geometry of a GNR with two ELDs. We denote this structure as 2ELD-ZGNR(n_1, n_2, n_3), where n_1, n_2, and n_3 denote the number of zigzag carbon lines above, within, and below the line defects. Figure 1(f) shows the electronic structure of the 2ELD-ZGNR(8,4,8). In this case, two additional bands are introduced near the Fermi level, as noted by the thick lines (in red). In this structure, the asymmetry between electron and hole bands around the Fermi level ($E=0$ eV) is further enhanced.

a. 1st design parameter—the effect of ELD. Fig. 2 demonstrates the increase in the asymmetry of the bands around the Fermi level by showing how the transmission changes when one or two ELDs are introduced in the channel. For the pristine ZGNR, the transmission is equal to one, indicating the existence of a single propagating band at energies around the Fermi level, denoted "Pristine" (green line). With the introduction of one ELD, the

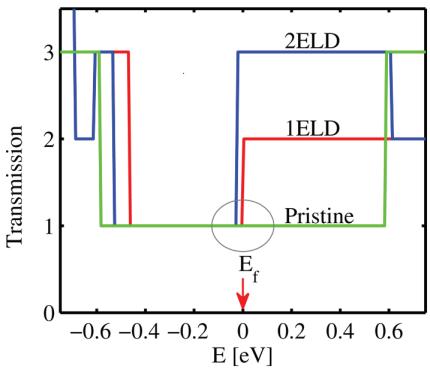

FIG. 2. (Color online) The transmission function for three different structures: i) the pristine ZGNR(20), ii) ELD-ZGNR(10,10), and iii) 2ELD-ZGNR(8,4,8).

conduction band ($E > 0$ eV) is composed of two subbands, whereas the valence band ($E < 0$ eV) is still composed of one subband. With the introduction of two ELDs, three conduction subbands now appear, but still only one valence subband. As it will be shown below, this asymmetry will improve the Seebeck coefficient. This constitutes the first design step in improving the thermoelectric performance of ZGNRs.

There is, however, another point worth mentioning. In Fig. 3, we show color maps of the normalized current spectrum at $E = 0.2$ eV in the cross sections of the ELD-ZGNRs described in Fig. 2. Figure 3(a) shows the current spectrum of the ELD-ZGNR(10,10). The current is zero close to the edges of the ribbon and peaks near the center. This is demonstrated more clearly in Fig. 3(d), which shows the current along one atomic chain perpendicular to this channel (ELD-blue line). The Pristine-black line of Fig. 3(d) illustrates the current density on the cross section of the pristine ZGNR channel for reference.

The current spectrum for the 2ELD-ZGNR(8,4,8) is shown in Fig. 3(b). The situation is now different, since most of the current is confined within the two ELDs. This, however, is the case only when the distance between the ELDs is smaller than the widths of the upper/lower regions. In the case where the width of the middle region is similar to the widths of the upper/lower regions, the current is spread more uniformly in the channel, as shown in Fig. 3(c) for the 2ELD-ZGNR(7,6,7) channel. Figure 3(e) shows again the current along one atomic chain in the cross section of these the ribbons. The current spectrum is localized in the middle of the channel in the 2ELD-ZGNR(8,4,8) channel (line "2" - red) compared to the pristine channel (line "P" - black). In a 2ELD-ZGNR(9,2,9) channel with a narrower middle region, the current spectrum is localized even closer around the center (line "1" - blue). A large portion of the current is, in general, flowing around the ELD regions. The design capability to localize the current spectrum in the middle of the channel away from the edges will prove advantageous in the presence of edge roughness, since the current in this case will be less affected. On the other hand, in the case of the 2ELD-ZGNR(7,6,7) channel, the current spectrum tends to concentrate more close to the edges (line "3" - green).

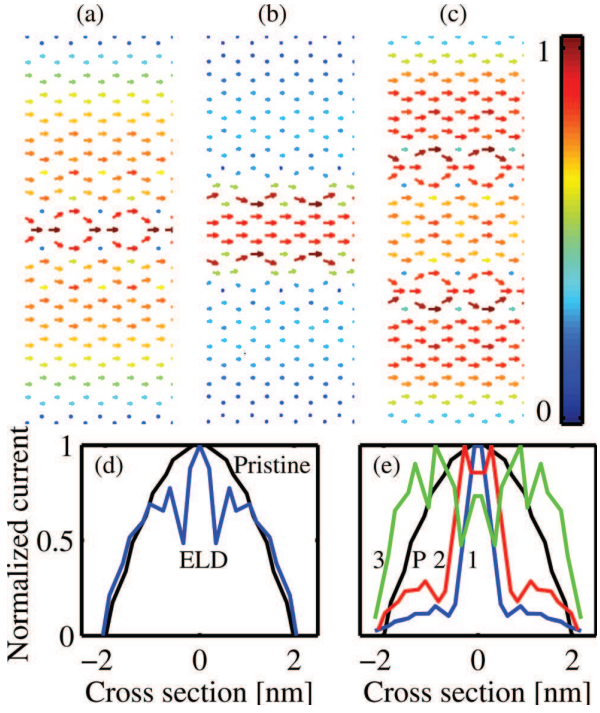

FIG. 3. (Color online) Normalized current spectrum at $E = 0.2$ eV for (a) ELD-ZGNR(10,10), (b) 2ELD- ZGNR(8,4,8), and (c) 2ELD(7,6,7). (d) The current in the cross section of ZGNR(20) denoted "Pristine" (black) and ELD-ZGNR(10,10) denoted ELD (blue). (e) The current in the cross section of ZGNR(20) denoted "P" (black), 2ELD-ZGNR(9,2,9) denoted "1" (blue), 2ELD-ZGNR(8,4,8) denoted "2" (red), and 2ELD-ZGNR(7,6,7) denoted "3" (green).

b. 2nd design parameter—the effect of background positive impurities. We next illustrate the possibility of further enhancing the asymmetry between electron and hole transport near the Fermi level by the introduction of positively charged substrate background impurities. The effect of background impurities is included in the Hamiltonian in a simplified way as an effective negative long range potential energy on the appropriate on-site Hamiltonian elements, as described in Ref. 19. A positive impurity in the substrate will constitute a repulsive potential for holes (a barrier for holes, but a well for electrons) and will degrade hole transport more effectively than electron transport. Figure 4(a) shows how the transmission of the ELD-ZGNR(10,10) channel (dashed-black line) is affected after the introduction of positive charged impurities in the channel (solid-blue line). Indeed, the transmission of holes below the Fermi level ($E = 0$ eV) is degraded. This effect additionally increases the asymmetry of the propagating bands and improves the Seebeck coefficient. On the other hand, the opposite is observed when negative impurities are introduced in the substrate. Negative impurities are a barrier for electrons and reduce their transmission,[34] but do not interfere with the hole subsystem, as shown in Fig. 4(b). This type of impurities will actually harm the asymmetry and needs to be avoided.

c. 3rd design parameter—the effect of roughness. In the third step of the design process, we introduce the effect of edge roughness. The inset of Fig. 4(c) shows the influence of edge roughness on the transmission of the ZGNR(20) of

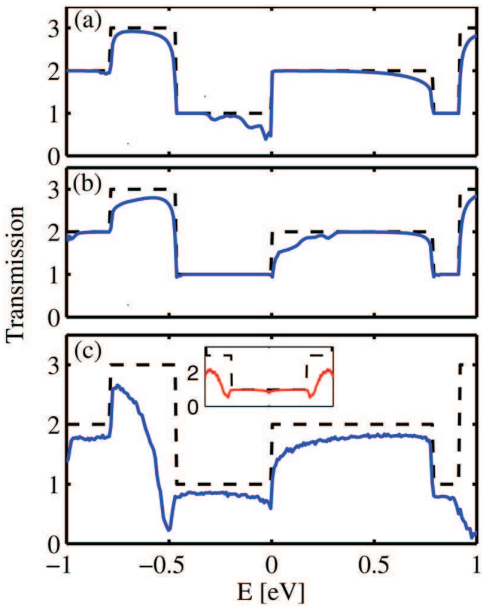

FIG. 4. (Color online) The effect of (a) positive substrate impurity, (b) negative substrate impurity, and (c) roughness on the transmission of ELD-ZGNR(10,10) with length of 125 nm. Inset of (c): The transmission of ZGNR(20) in the presence of roughness.

length 125 nm. As also described in previous studies,[15,19] in the first conduction plateau the effect is negligible. In contrast to ZGNR, ELD-ZGNRs as well as 2ELD-ZGNRs are affected by edge roughness. This is because the band structure of these GNRs has undergone a band folding, and therefore, the states in the first conduction plateau have smaller wave vectors. As the long range defects can induce only small value of momentum transfer, the momentum conservation rule indicates that, in contrast to the ZGNR, the transport of ELD-ZGNRs and 2ELD-ZGNRs will be more affected and will not remain ballistic in the presence of line edge roughness and long range substrate impurities. This is shown in Fig. 4(c), where the transmission of a roughened 125-nm-long ELD-ZGNR(10,10) channel (solid-blue line) is reduced by ~25% compared to the ballistic value (dashed-black line). Edge roughness degrades the conductivity of holes and electrons by a similar amount, and therefore, the level of asymmetry around the Fermi level is retained.

Figures 5(a) and 5(b) illustrate the influence of roughness in ELD-ZGNR channels on their transmission, for channels of different lengths and widths. In this calculation, positive impurities are also included. Figure 5(a) shows the transmission of edge-roughened ELD-ZGNR(10,10) versus energy for the channel lengths $L = 250$, 500, and 2000 nm. As the channel length is increased, the transmission drops further compared to the transmission of the ideal channel (black solid line). This is expected, since the channel resistance increases with increasing length. Figure 5(b) illustrates the effect of the ribbon's width on the transmission of ELD-ZGNRs with rough edges. In this case, the length is kept constant at $L = 250$ nm, and results for three different ribbon with parameters (10,10), (7,7), and (5,5) are shown. As the width of the ribbon is decreased, the effect of line edge roughness scattering on the transmission becomes stronger, because the carriers reside on average closer to the edges.

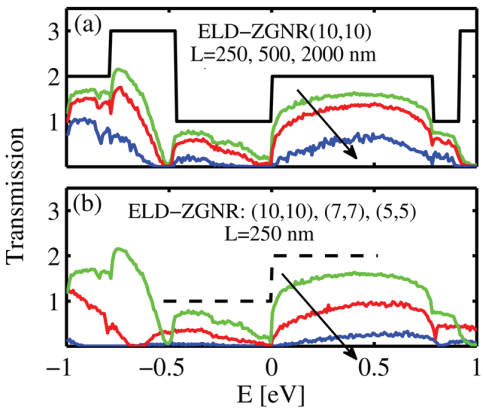

FIG. 5. (Color online) The influence of roughness and positive impurities on the ELD-ZGNR channel. (a) Electronic transmission of ELD-ZGNR(10,10). Rough edges are assumed and the length L is varied. The arrow indicates increasing values of length L. (b) Electronic transmission of ELD-ZGNRs with different widths. The length is assumed to be constant at 250 nm and the arrow indicates the direction of decreasing the ribbon's width. Black solid and black dashed lines in (a) and (b): The transmission of the pristine ELD-ZGNR.

It is worth mentioning that the effect of edge roughness on the transmission is much stronger in AGNR than in ZGNR. Although, in the case of some AGNRs, a bandgap is naturally present and the asymmetry does not need to be created with the introduction of line defects and impurities, the conductance is severely degraded by the roughness, which renders this type of ribbon not well suited for transport applications.[19] (Note that edge roughness will be needed in order to reduce thermal conductivity, as will be shown below.)

As we mentioned above in Fig. 3, the channel which includes two ELDs can shift the majority of the current spectrum in the region between the two ELDs and, thus, farther away from the edges. It is, therefore, expected that the 2ELD-ZGNR will be less affected by edge roughness scattering than the ELD-ZGNR. A comparison of the transmission of these devices with rough edges is shown in Fig. 6. The transmission of ELD-ZGNR(n_1,n_1) and two cases of 2ELD-ZGNR, 2ELD-ZGNR(n_2,4,n_2) and the 2ELD-ZGNR(n_3,6,n_3) at $E = 0.2$ eV versus their width W, are compared. The parameters n_i are adjusted such that the three channels have nearly the same width W. The first channel belongs to the category shown in Fig. 3(a), the second in the category of Fig. 3(b), and the third in the category of Fig. 3(c). The third channel, as shown in Fig. 3, spreads the current spectrum more uniformly in the channel and is expected to be affected the most from edge roughness. All channels have the same length of $L = 250$ nm. For smaller widths, the effect of roughness is strong and the transmissions of all channels are drastically reduced. Since the 2ELD-ZGNR devices can concentrate the current spectrum around the defect lines, as shown in Figs. 3(b) and 3(c), they effectively bring it closer to the edges, and the reduction is larger for these devices. For larger widths, the transmission of the ribbons approaches its ballistic value, which is 2 for the ELD-ZGNR devices and 3 for the 2ELD-ZGNR devices. The transmission of the 2ELD-ZGNR(n_2,4,n_2) channels increases faster with increasing channel width, because the current spectrum is located farther from the edges, which

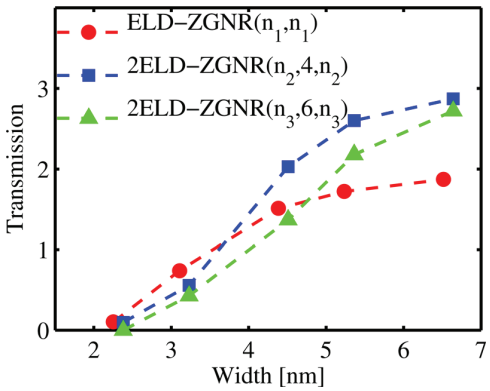

FIG. 6. (Color online) Transmission at $E = 0.2$ eV for three different structures as indicated vs their width. The length is assumed to be constant at 250 nm.

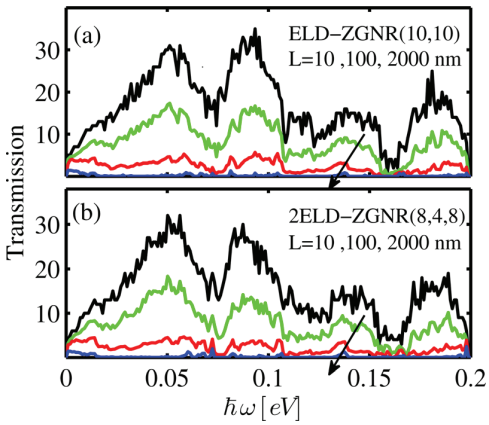

FIG. 7. (Color online) Phonon transmission probability of (a) ELD-ZGNR(10,10) and (b) 2ELD-ZGNR(8,4,8). Rough edges are assumed, and the length L of the channel is varied. Upper lines (black): The phonon transmission of the channels with line defects, but without roughness. Lower three lines: The arrows indicate increasing values of channel length L: 10 nm (green), 100 nm (red), 2000 nm (blue).

makes it less susceptible to scattering as the width increases. The transmission of the 2ELD-ZGNR(n_3,6,n_3) channel eventually increases close to the ballistic transmission value as the width increases, but it increases more slowly than that of the 2ELD-ZGNR(n_2,4,n_2) channel.

d. Effect of roughness on phonon transport. Although the reduction in the electronic transmission of channels with ELDs can be quite strong when considering edge roughness, the reduction in the lattice part of the thermal conductivity is even stronger. We take advantage of this effect when attempting to optimize the thermoelectric figure of merit. The phonon transmission for the edge-roughened ELD-ZGNR(10,10) channel versus energy is shown in Fig. 7(a). Results for channel lengths $L = 10$, 100, and 2000 nm are shown. As expected, the transmission decreases as the length is increased. What is important, however, is that the decrease is much stronger than the decrease of the electron transmission shown in Fig. 5(a).

For example, for a channel length of $L = 100$ nm, the phonon transmission reduces by more than a factor of 6X, whereas the electronic transmission even at larger length $L = 250$ nm reduces only by $<30\%$. Interestingly, the same order of reduction of the phonon transmission is observed for the 2ELD-ZGNRs, as shown in Fig. 7(b), indicating that the line defect does not affect phonon conduction significantly compared to the effect of edge roughness.

B. Thermoelectric coefficients

The denominator of the ZT figure of merit consists of the summation of the contributions to the thermal conductivity of the electronic system and the phononic system. In graphene, the phonon part dominates the thermal conductivity, whereas the electronic part contribution is much smaller. The situation is different, however, in rough ELD-ZGNRs, in which the phonon thermal conductivity is degraded more than the electronic thermal conductivity. Figure 8 clearly illustrates this effect by showing the ratio of the phonon thermal conductance to the electronic thermal conductance versus the rough channel length. The cases of ELD-ZGNR(10,10) and 2ELD-ZGNR(8,4,8) are shown in dashed red and dashed-dot blue lines, respectively. For small channel lengths, where transport is quasi-ballistic and roughness does not affect the transmission significantly, κ_l is almost 5X larger than κ_e. As the length of the channel increases and the effect of the roughness becomes significant, the phonon system is degraded more than the electronic system, and the κ_l is significantly reduced compared to κ_e. For lengths $L \sim 100$ nm and beyond, κ_l can become even smaller than κ_e. The trend is the same when considering channels with one or two ELDs. We note that from the inset of Fig. 8 which shows that the ratio of the electrical conductance G over κ_e is almost constant, it can be indicated that both G and κ_e follow the same trend, as the Wiedemann-Franz law dictates. We mention that the κ_l and κ_e values used in Fig. 7 are extracted using the corresponding mean free paths (MFPs) for phonons and electrons, respectively, defined as described in Ref. 15,

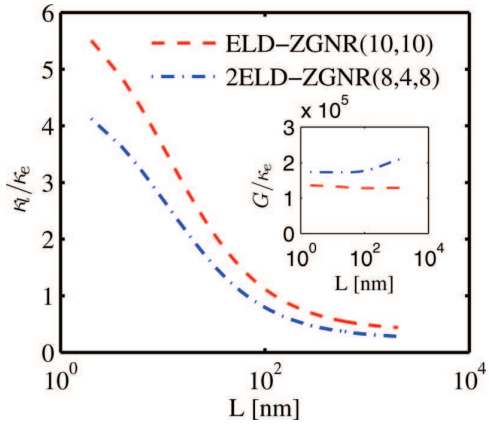

FIG. 8. (Color online) The ratio of the phononic to the electronic thermal conductivity vs channel length L for the ELD and 2ELD structures as noted. Inset: The ratio of the electronic conductivity to the electronic part of the thermal conductivity vs channel length L.

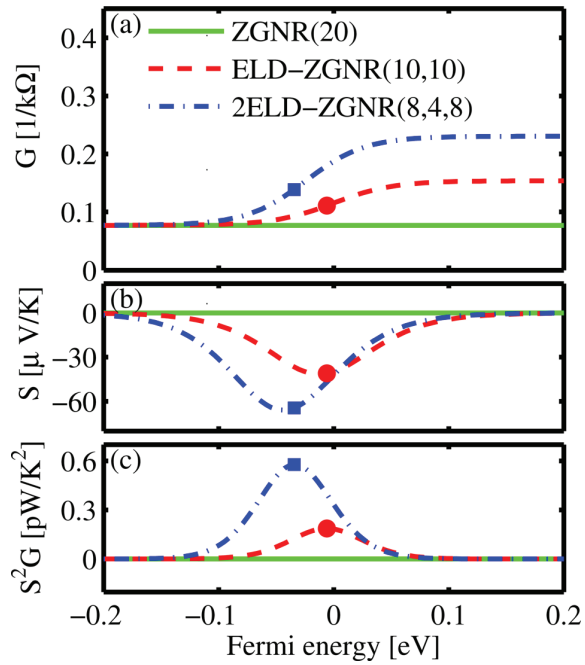

FIG. 9. (Color online) (a) Electrical conductance, (b) Seebeck coefficient, and (c) thermoelectric power factor of pristine ZGNR(20), ELD-ZGNR(10,10), and 2ELD-ZGNR(8,4,8) channels with perfect edges. The dots indicate the Fermi energy values at which the peak of the power factor occurs for the ELD and 2ELD channels.

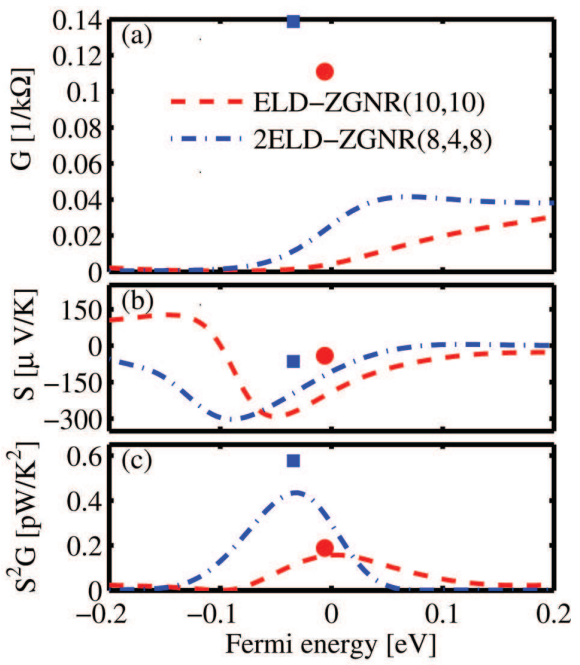

FIG. 10. (Color online) (a) Electrical conductance, (b) Seebeck coefficient, and (c) thermoelectric power factor of ELD-ZGNR(10,10) and 2ELD-ZGNR(8,4,8) with rough edges and positively charged substrate impurities. The channel length is 2 μm. The dots indicate the Fermi energy values at which the peak of the power factor occurs for the pristine ELD and 2ELD channels of Fig. 9 for comparison purposes.

$$T(E) = \frac{N_{ch}(E)}{1 + \frac{L}{\lambda(E)}}, \tag{10}$$

where $T(E)$ is transmission probability, $N_{ch}(E)$ is the number of modes at energy E, L is the given length of the channel, and $\lambda(E)$ is the mean free path of the carriers. Alternatively, κ_l and κ_e could be extracted from the transmission calculations by using a statistical average over several rough samples for each channel length. The results of both methodologies are in good agreement for the electronic part of the thermal conductivity. For the lattice part, the agreement is good only for the shorter channels below ~100 nm. For larger channel lengths, the phonon transmission is severely reduced, which increases the noise in the calculation for extracting the κ_l. The values extracted directly from the integration of the phonon transmission could be as much as $2X$ larger, which could increase the κ_l/κ_e by a factor of $2X$ for the longer channels. In this case, the ratio κ_l/κ_e will be closer to unity, but this is still a huge advantage compared to devices without roughness.

a. Power factor. Using the first design step, i.e., the effect of ELDs, we have demonstrated that the transmission of electrons around the Fermi level can be increased (from $T=1$ to $T=2$ and $T=3$ in the presence of one and two ELDs, respectively). An asymmetry is thus created between holes and electrons. This increases both the conductivity and Seebeck coefficient of the channel, as shown in Fig. 9. Figure 9(a) shows the conductance of the 2ELD-ZGNR (8,4,8) (dashed-dot-blue), of the ELD-ZGNR (10,10) (dashed-red), and of the pristine nanoribbon (green) at room temperature, 300 K. As expected, the conductance of the channel with two ELDs is the largest, followed by the channel with one ELD. They are larger than the pristine channel by ~$3X$ and ~$2X$, respectively. Figure 9(b) shows the changes of the Seebeck coefficient after the introduction of the ELDs in the nanoribbon. Due to its metallic behavior and the flat transmission near the Fermi level, the pristine channel exhibits zero Seebeck coefficient. Due to the built asymmetry after the introduction of the ELDs, however, the Seebeck coefficient increases for both channels. The channel with two line defects has the largest asymmetry and, therefore, the largest Seebeck coefficient (in absolute values). Finally, the power factor in Fig. 9(c) is, indeed, largely improved in the ELD structures and especially the 2ELD-ZGNR channel.

In Fig. 10 we show the same thermoelectric coefficients for the same structures as in Fig. 9, but now edge roughness and positive impurities are included in the calculation. The length of the channels in this case is 2000 nm. A similar qualitative behavior is observed as in Fig. 9 for both channels. Quantitatively, however, the conductance in Fig. 10(a) is now significantly reduced by a factor of ~$15X$ (the dots correspond to the position of the peak of the power factor of the devices without roughness and impurities in Fig. 9). The Seebeck coefficient in Fig. 10(b), on the other hand, increases. Finally, the peak of the power factor in Fig. 10(c) reduces only slightly compared to the peak of the power factor of the devices without edge roughness in Fig. 9(c) (dots).

b. Thermoelectric figure of merit. For the devices that include rough edges, however, as we demonstrated in Fig. 8,

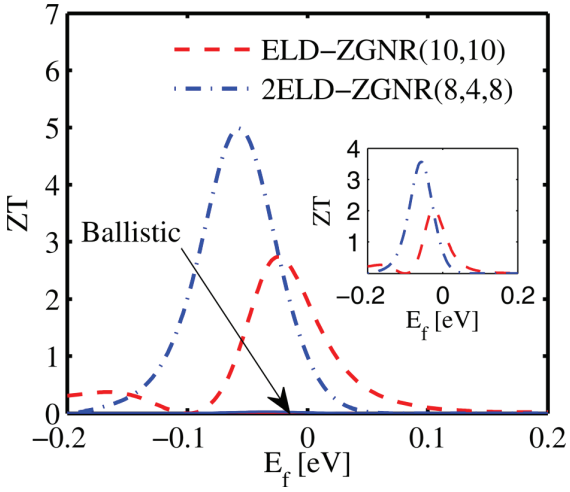

FIG. 11. (Color online) The thermoelectric figure of merit *ZT* for the ELD-ZGNR(10,10) (dashed red line) and 2ELD-ZGNR(8,4,8) (dashed-dot blue line) channels of length $L = 2$ μm. The lattice thermal conductance is extracted from the calculated mean free path. Inset: The same figure of merit *ZT*, but with the lattice thermal conductance extracted by integrating the simulated phonon transmission.

the phonon thermal conductivity is drastically reduced compared to the electronic thermal conductivity. A large improvement is, therefore, expected in the *ZT* figure of merit. Figure 11 shows the *ZT* figure of merit versus energy at room temperature for the ELD-ZGNR(10,10) (denoted "Ballistic"), the ELD-ZGNR(10,10) with impurities and roughness (dashed-red), and the 2ELD-ZGNR(8,4,8) (dashed-dot-blue) with impurities and roughness. As indicated, large values of *ZT* can be achieved, especially in the case of the device with two ELDs. The phonon lattice conductivity value used in this calculation was extracted using the MFP method. Since, as explained above, that value could be 2*X* lower than the value extracted from direct integration of the "noisy" transmission, in the inset of Fig. 11, we show the *ZT* versus energy using the κ_l values extracted from the transmission. Indeed, the *ZT* could be reduced by a factor of $\sim 2X$, but still peak *ZT* values above 2 can be achieved at room temperature, which is comparable and even better than the best thermoelectric materials to date.[35] We note that, as shown by Ref. 15, rough ZGNRs can have high *ZT* values, even without the presence of ELDs. For this, however, the asymmetry in the sharp edges of the higher subbands is utilized at energies above 0.5 eV. Those energies, however, are too high and cannot easily be reached. Finally, we mention here that our formalism has considered scattering only by edge roughness and impurity scattering, whereas phonon scattering and dephasing mechanisms are not included. However, as it is shown for 1D NWs,[36] the effects of impurity scattering and edge roughness are the most important scattering effects in channels of cross sections below 5 nm, and we expect this to hold also for GNRs as well.

IV. SUMMARY

In this work, we present a theoretical design procedure for achieving high thermoelectric performance in zigzag graphene nanoribbon (ZGNR) channels, which, in their pristine form, have very poor performance. The fully quantum mechanical non-equilibrium Green's function technique was used for electron and phonon transport, and tight-binding and force constant methods were used for the electronic and phonon bandstructure descriptions. We show that, by introducing extended line defects (ELDs) in the length of the nanoribbon we can create an asymmetry in the density of modes around the Fermi level, which improves the Seebeck coefficient. ELDs increase the electronic conduction modes, which increase the channel conductance as well. The power factor is, therefore, significantly increased. In addition, we show that by introducing edge roughness the phonon thermal conductivity (κ_l) is drastically degraded much more than the electronic thermal conductivity (κ_e) or the electronic conductance (G). These three effects result in large values of the thermoelectric figure of merit and indicate that roughed ZGNRs with ELDs could potentially be used as efficient high performance thermoelectric materials.

ACKNOWLEDGMENTS

This work, as part of the ESF EUROCORES program EuroGRAPHENE, was partly supported by funds from FWF, Contract I420-N16. This work was also partly supported by the Austrian Climate and Energy Fund, Contract No. 825467.

[1]G. Nolas, J. Sharp, and H. Goldsmid, *Thermoelectrics: Basic Principles and New Materials Developments* (Springer, Germany, 2001).
[2]A. Hochbaum, R. Chen, R. Delgado, W. Liang, E. Garnett, M. Najarian, A. Majumdar, and P. Yang, Nature **451**, 163 (2008).
[3]A. Boukai, Y. Bunimovich, J. Tahir-Kheli, J.-K. Yu, W. Goddard, and J. Heath, Nature **451**, 168 (2008).
[4]R. Venkatasubramanian, E. Siivola, T. Colpitts, and B. O'Quinn, Nature **413**, 597 (2001).
[5]W. Kim, S. L. Singer, A. Majumdar, D. Vashaee, Z. Bian, A. Shakouri, G. Zeng, J. E. Bowers, J. M. O. Zide, and A. C. Gossard, Appl. Phys. Lett. **88**, 242107 (2006).
[6]J. Tang, H.-T. Wang, D. H. Lee, M. Fardy, Z. Huo, T. P. Russell, and P. Yang, Nano Lett. **10**, 4279 (2010).
[7]K. Novoselov, A. Geim, S. Morozov, D. Jiang, Y. Zhang, S. Dubonos, and I. Grigorieva, Science **306**, 666 (2004).
[8]J.-H. Chen, C. Jang, S. Xiao, M. Ishighami, and M. Fuhrer, Nature Nanotech. **3**, 206 (2008).
[9]S. Ghosh, I. Calizo, D. Teweldebrahn, E. Pokatilov, D. Nika, A. Balandin, W. Bao, F. Miao, and C. Lau, Appl. Phys. Lett. **92**, 151911 (2008).
[10]J. H. Seol, I. Jo, A. L. Moore, L. Lindsay, Z. H. Aitken, M. T. Pettes, X. Li, Z. Yao, R. Huang, D. Broido, N. Mingo, R. S. Ruoff, and L. Shi, Science **328**, 213 (2010).
[11]J. Hone, M. Whitney, C. Piskoti, and A. Zettl, Phys. Rev. B **59**, R2514 (1999).
[12]A. Balandin, S. Ghosh, W. Bao, I. Calizo, D. Teweldebrhan, F. Miao, and C. Lau, Nano Lett. **8**, 902 (2008).
[13]J.-W. Jiang, B.-S. Wang, and J.-S Wang, Appl. Phys. Lett. **98**, 113114 (2011).
[14]J. Hu, S. Schiffli, A. Vallabhaneni, X. Ruan, and Y. Che, Appl. Phys. Lett. **97**, 133107 (2010).
[15]H. Sevincli and G. Cuniberti, Phys. Rev. B **81**, 113401 (2010).
[16]M. Han, B. Ozyilmaz, Y. Zhang, and P. Kim, Phys. Rev. Lett. **98**, 206805 (2007).
[17]A. Zhang, H. Teoh, Z. Dai, Y. Feng, and C. Zhang, Appl. Phys. Lett. **98**, 023105 (2011).
[18]Y. Ouyang and J. Guo, Appl. Phys. Lett. **94**, 263107 (2009).
[19]D. Areshkin, D. Gunlycke, and C. White, Nano Lett. **7**, 204 (2007).
[20]D. Bahamon, A. Pereira, and P. Schulz, Phys. Rev. B **83**, 155436 (2011).
[21]R. Kim, S. Datta, and M. S. Lundstrom, J. Appl. Phys. **105**, 034506 (2009).
[22]C. Jeong, R. Kim, M. Luisier, S. Datta, and M. Lundstrom, J. Appl. Phys. **107**, 023707 (2010).

[23]H. Karamitaheri, M. Pourfath, R. Faez, and H. Kosina, J. Appl. Phys. **110**, 054506 (2011).
[24]C. Jeong, S. Datta, and M. Lundstrom, J. Appl. Phys. **109**, 073718 (2011).
[25]J. Lahiri, Y. Lin, P. Bozkurt, I. I. Oleynik, and M. Batzill, Nature Nanotech. **5**, 326 (2010).
[26]D. J. Appelhans, L. D. Carr, and M. T. Lusk, New J. Phys. **12**, 125006 (2010).
[27]M. T. Lusk, D. T. Wu, and L. D. Carr, Phys. Rev. B **81**, 155444 (2010).
[28]R. Saito, M. Dresselhaus, and G. Dresselhaus, *Physical Properties of Carbon Nanotubes* (Imperial College Press, London, 1998).
[29]M. U. Kahaly, S. P. Singh, and U. V. Waghmare, Small **4**, 2209 (2008).
[30]H. Karamitaheri, N. Neophytou, M. Pourfath, and H. Kosina, "Study of thermal properties of graphene-based structures using the force constant method" J. Comput. Electron. (in press) (to be published).
[31]M. Sancho, J. Sancho, J. Sancho, and J. Rubio, J. Phys. F: Met. Phys. **15**, 851 (1985).
[32]S. Datta, *Quantum Transport: Atom to Transistor* (Cambridge University Press, Cambridge, 2005).
[33]V. M. Pereira, F. Guinea, J. M. B. L. dos Santos, N. M. R. Peres, and A. H. C. Neto, Phys. Rev. Lett. **96**, 036801 (2006).
[34]N. Neophytou, D. Kienle, E. Polizzi, and M. P. Anantram, Appl. Phys. Lett. **88**, 242106 (2006).
[35]G. J. Snyder and E. S. Toberer, Nature Mater. **7**, 105 (2008).
[36]N. Neophytou and H. Kosina, Phys. Rev. B **83**, 245305 (2011).